Unitarity Triangles at *BABAR*

Fernando Martínez-Vidal[a], representing the *BABAR* Collaboration

[a]Instituto de Física Corpuscular (IFIC), Universitat de València-CSIC,
Apartado de Correos 22085, E-46071 Valencia, Spain

The *BABAR* experiment has used a variety of methods to determine the angles α, β, and γ of the Cabibbo-Kobayashi-Maskawa Unitarity Triangle, which give insight into the Standard Model description of *CP* violation in the quark sector of the electroweak interactions. Here we review the main experimental techniques and analyses, with emphasis in the most recent results [1].

1. INTRODUCTION

In the Standard Model (SM), the Cabibbo-Kobayashi-Maskawa (CKM) matrix $V_{\rm CKM}$ [2] mixes (left-handed) down-quark mass eigenstates to give down-quark weak (physical) eigenstates, and thus describes the complex couplings of the charged weak current to quarks. The unitarity of the 3×3 matrix leads to six unitarity conditions and leaves only one irreducible phase, which is the sole origin of *CP* violation in the SM. In the Wolfenstein parameterization [3],

$$V = \begin{pmatrix} 1-\frac{\lambda_C^2}{2} & \lambda_C & A\lambda_C^3(\rho - i\eta) \\ -\lambda_C & 1-\frac{\lambda_C^2}{2} & A\lambda_C^2 \\ A\lambda_C^3(1-\rho-i\eta) & -A\lambda_C^2 & 1 \end{pmatrix}$$

valid to $\emptyset(\lambda_C^4)$, where $\lambda_C \approx \sin\theta_C$ (Cabibbo angle), this phase appears in the V_{ub} and V_{td} elements. One unitarity condition, $V_{ud}V_{ub}^* + V_{cd}V_{cb}^* + V_{td}V_{tb}^* = 0$, can be represented as a triangle of roughly equal-length sides, as shown in Fig. 1, and it is usually referred as the Unitarity Triangle. In this triangle, the angle between the V_{ub} and V_{cb} sides is known as γ, and the angle between the V_{td} and V_{cb} sides as β. The third angle α is trivially related to β and γ, $\alpha + \beta + \gamma = \pi$. Therefore, in the Wolfenstein representation $\gamma = -\mathrm{Arg}(V_{ub})$ and $\beta = -\mathrm{Arg}(V_{td})$.

Here we review the main analysis techniques and recent results of the angles β and α obtained by measuring time-dependent *CP* asymmetries, and the newest results of the angle γ obtained by determining direct *CP* asymmetries,

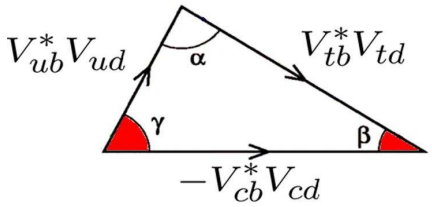

Figure 1. Graphical representation of the unitarity condition $V_{ud}V_{ub}^* + V_{cd}V_{cb}^* + V_{td}V_{tb}^* = 0$.

performed by the *BABAR* experiment [4,5] at the PEP-II asymmetric-energy e^+e^- collider. The *BABAR* experiment has recorded 433 fb^{-1} of data at the $\Upsilon(4S)$ resonance[1]. Nevertheless, most of the analyses reported here make use of 350 fb^{-1}, unless otherwise specified.

2. EXPERIMENTAL TECHNIQUES

The determination of the CKM phases requires to measure rates for *CP* conjugate processes in decays where there are two paths to reach the same final state, provided that the relative strong phase does not vanish. A text book example is the interference via mixing between B^0 and $\overline{B}^0$ mesons decaying to $J/\psi K_S^0$ in the final state, which allow the determination of the angle β. Here, the first path is provided by the decay of a B^0 meson into the final state, and the second path by the oscillation to a $\overline{B}^0$ meson and its subsequent decay to the same final state (Fig. 2). The decay is domi-

[1]Plus 30 fb^{-1} at the $\Upsilon(3S)$, 15 fb^{-1} at the $\Upsilon(2S)$, and 54 fb^{-1} 30 MeV below the $\Upsilon(4S)$ resonance.

nated by a $b \to c\overline{c}s$ tree amplitude and a $b \to s\overline{c}c$ penguin amplitude. The latter has a contribution with c and t in the loop that has the same weak phase as the tree amplitude, and has also a second contribution with u and t in the loop with different weak phase but it is suppressed by λ_C^2 relative to the first contribution. Due to this suppression the direct decay has, to $\emptyset(\lambda_C^4)$, no weak phases. The mixing phase is 2β, since in the corresponding box diagram there are two occurrences of V_{td} (Fig. 2). The ratio of amplitudes

$$\lambda_f = \frac{\mathcal{A}(B^0 \to \overline{B}^0 \to f)}{\mathcal{A}(B^0 \to f)} = \frac{q}{p}\frac{\mathcal{A}(\overline{B}^0 \to f)}{\mathcal{A}(B^0 \to f)},$$

where q and p are the complex coefficients relating the flavor eigenstates B^0 and $\overline{B}^0$ to the mass eigenstates, is

$$\lambda_f = \eta_f \frac{V_{td}V_{tb}^*}{V_{td}^*V_{tb}} \frac{V_{cb}V_{cs}^*}{V_{cb}^*V_{cs}} \frac{V_{cd}^*V_{cs}}{V_{cd}V_{cs}^*} = \eta_f e^{-i2\beta},$$

where $\eta_f = \pm 1$ is the CP eigenvalue of the final state f (-1 for $J/\psi K_S^0$). The last factor accounts for the K^0 oscillating to a K_S^0.

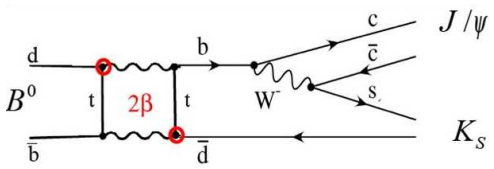

Figure 2. Main diagram contributing to the process $B^0 \to \overline{B}^0 \to J/\psi K_S^0$ interfering with the direct decay $B^0 \to J/\psi K_S^0$.

When we have neutral B decays, a time-dependent analysis is needed to disentangle the effects from mixing and decay. Experimentally we determine a sine ($\mathcal{S}$) and a cosine ($\mathcal{C}$) coefficient from a fit to the time dependent decay rate. The corresponding raw time dependent CP asymmetry is

$$\begin{aligned} \mathcal{A}_{CP,f}(\Delta t) &= \frac{\Gamma_{f,-}(\Delta t) - \Gamma_{f,+}(\Delta t)}{\Gamma_{f,-}(\Delta t) - \Gamma_{f,+}(\Delta t)} \\ &= \mathcal{S}_f \sin(\Delta m \Delta t) - \mathcal{C}_f \cos(\Delta m \Delta t). \end{aligned}$$

The CP violating coefficients $\mathcal{S}_f$ and $\mathcal{C}_f$ can then be related to the fundamental parameters describing the mixing and the decay, and therefore to the CKM angles. For $f = J/\psi K_S^0$ decays, $|\lambda_f| = 1$, $\mathcal{C}_f = (1 - |\lambda_f|^2)/(1 + |\lambda_f|^2) = 0$ and $\mathcal{S}_f = 2\Im\lambda_f/(1 + |\lambda_f|^2) = \sin 2\beta$. The deviation $\Delta S_f = S_f - \sin 2\beta$ due to the penguin pollution has been estimated to be at 10^{-3} level [6].

Time-dependent measurements start by fully reconstructing one of the two B mesons produced in the $\Upsilon(4S)$ decay. B candidates are characterized using two kinematic variables, the beam-energy substituted B mass $m_{\rm ES}$, and the energy difference in center-of-mass (CM) frame $\Delta E = E_B^* - \sqrt{s}/2$. The $m_{\rm ES}$ resolution ($\sim$ 2.6 MeV) is dominated by the beam energy spread, while the ΔE resolution depends on the charged and neutral multiplicity of the B decay, and ranges between 10 and 50 MeV.

A tagging algorithm [7] is then used to identify the flavor at production of the signal B (fully reconstructed B), i.e. whether it is B^0 or $\overline{B}^0$. This algorithm uses tracks from the rest of the event and exploits the coherent B meson production (P-wave) in the the $\Upsilon(4S)$ decay. The signal-side tracks are then fit to a decay vertex, and from the tagging-side tracks an optimal vertex is searched and fit. The distance Δz between the two vertices along the beam axis provides the time difference Δt between the B decays, $\Delta z \approx \beta\gamma c\Delta t$, where $\beta\gamma \approx 0.55$ is the Lorentz boost of the CM frame. For this boost, the average Δz is about 250 μm. High statistics data samples of self-tagging B^0 and $\overline{B}^0$ decays are used to calibrate the tagging and the time resolution. The calibrated tagging performance is $Q = \epsilon(1 - 2w)^2 \approx 30\%$ (ϵ and ω denote the tagging efficiency and mistag rate, respectively), and the Δz resolution (rms) is about 170 μm ($\sim$ 1 ps on Δt), largely dominated by the tagging-side vertex.

The dominant background is typically $e^+e^- \to q\overline{q}$ ($q = u, d, s, c$) continuum events. Suppression and characterization of these events are performed using event shape variables, combined using multivariate methods. Fisher discriminants are an usual choice, combining different topological variables which account for the jet-like shape of continuum events, in comparison to the spher-

ical topology of $B\overline{B}$ events, as well as variables accounting for the differences in the angular distribution of signal B candidates with respect to background.

In addition, most analyses apply selection cuts (vetoes) to reduce potentially dangerous B decay backgrounds. Depending on the decay channel under consideration, these vetoes can be based on intermediate resonance masses, decay angles, helicity in $P \to PV$ and $V \to PP$ decays, and particle identification.

Finally, maximum likelihood fits are performed to a subset of discriminating variables (e.g. $m_{\rm ES}$, ΔE, Fisher, particle identification, Δt, tagging, etc.) to extract signal and background parameters. The use of sidebands and control samples provides a robust determination of backgrounds and cross-checks on data.

3. MEASURING β

This angle is the most accurately measured using $b \to c\overline{c}s$ transitions. This measurement [8] includes $B^0 \to J/\psi K^0_S$, $\psi(2S)K^0_S$, $\chi_{c1}K^0_S$, $\eta_c K^0_S$, $J/\psi K^{*0}$ ($K^{*0} \to K^0_S\pi^0$), and $J/\psi K^0_L$ decays; we use $B^0 \to J/\psi K^0$ to refer generally to all the six modes, and $B^0 \to J/\psi K^0_S$ to denote all the first five modes. The fit to the B^0 and $\overline{B}^0$ Δt distributions yields $\sin 2\beta = 0.714 \pm 0.032 \pm 0.018$ (3.5% total error), yet dominated by the statistical uncertainty, and $|\lambda| = 0.952 \pm 0.022 \pm 0.017$, both in agreement with the theoretical expectation. Here and thereafter the first error is statistical and the second is the systematic uncertainty.

The angle β can also be measured using $b \to c\overline{c}d$ and $b \to q\overline{q}s$, with $q = d, s$, transitions. Decays involving $b \to c\overline{c}d$ (e.g. $B^0 \to J/\psi\pi^0$, $D^{(*)+}D^{(*)-}$) and $b \to d\overline{d}s$ (e.g. $B^0 \to \eta' K^0$, ωK^0, $\pi^0 K^0$, $\rho_0 K^0$, $f_0 K^0$) transitions are dominated by penguin amplitudes, while $b \to s\overline{s}s$ processes (e.g. $B^0 \to \phi K^0$, $K^+K^-K^0$, $K^0K^0K^0$) proceed exclusively via penguin amplitudes. All these have the same weak phase as the $b \to c\overline{c}s$ tree amplitude, since the penguin loop factorizes into a c, t loop with the same weak phase and a u, t loop with a different weak phase but suppressed by λ^2_C relative to $b \to c\overline{c}s$ (see Fig. 3). Thus we expect for these decays $\mathcal{C}_f = 0$ and $\mathcal{S}_f = \sin 2\beta$, with mode-dependent corrections (below $\sim 20\%$, relatively small compared to the current experimental errors) to this prediction due to SM hadronic corrections (final-state rescattering) [9]. Since the penguin dominated processes $b \to q\overline{q}s$ involve only flavor-changing neutral currents (no interference between tree and penguin diagrams, resulting in negligible *CP* violation), they are particularly sensitive to new physics beyond the SM contributing to the loops, which would manifest through deviations of $\mathcal{S}_f$ from the reference $\sin 2\beta$ as measured in $b \to c\overline{c}s$ transitions.

An example of $b \to c\overline{c}d$ transition recently updated using the complete data sample recorded by *BABAR* is the $J/\psi\pi^0$ final state. The fit to the B^0 and $\overline{B}^0$ Δt distributions yields $\mathcal{S}_{J/\psi\pi^0} = -1.23 \pm 0.21 \pm 0.04$ and $\mathcal{C}_{J/\psi\pi^0} = -0.20 \pm 0.19 \pm 0.03$ [10]. The $\mathcal{S}_{J/\psi\pi^0}$ coefficient has a significance of 4.0 standard deviations, thus implying strong evidence of *CP* violation in this decay, and compared to the reference from $B^0 \to J/\psi K^0$ decays is about 2.5 standard deviations away. This channel is interesting since it provides a data driven avenue to constraint the penguin correction in $B^0 \to J/\psi K^0$ [11], leading to a negligible $\Delta S_{J/\psi K^0_S}$ correction with an uncertainty at 1% level, dominated by the errors on $\mathcal{S}, \mathcal{C}_{J/\psi\pi^0}$. Measurements in other $b \to c\overline{c}d$ decays, like $B^0 \to D^{(*)+}D^{(*)-}$ [12] are consistent with the reference.

There are no recent updates on measurements involving $b \to q\overline{q}s$ transitions. All penguin modes tend to give $\mathcal{S}_f$ values lower than the reference from $B^0 \to J/\psi K^0$ modes [13], although the effect is not statistically significant. However, it is interesting to note that the offset mode by mode has in general a sign opposite to that obtained from the SM hadronic corrections [9].

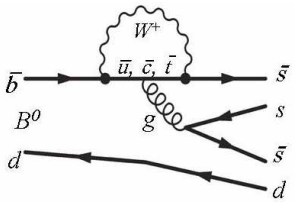

Figure 3. Penguin diagram contributing to $b \to s\overline{s}s$ transitions.

4. MEASURING α

The angle α can be measured from the interference between direct and B^0-$\overline{B}^0$ mixing induced $b \to u\overline{u}d$ decays, as illustrated in Fig. 4. This is obtained by fitting the Δt distribution in decays of neutral B decays into $\pi^+\pi^-$, $\rho^+\rho^-$, and $\rho^+\pi^-$ final states (referred to hereafter collectively as h^+h^-). If only $b \to u\overline{u}d$ transitions were present in these decays, the ratio of decay amplitudes would be $\lambda_f = \eta_f[V_{td}V_{tb}^*]/[V_{td}^*V_{tb}][V_{ub}V_{ud}^*]/[V_{ub}^*V_{ud}] = \eta_f e^{i2\alpha}$, and then $\mathcal{S}_f = \eta_f \sin\alpha$ and $\mathcal{C}_f = 0$. However, a $b \to d\overline{u}u$ penguin amplitude also contributes (see Fig. 4), and unlike the penguin in $B^0 \to J/\psi K^0$ decays, the piece with a different weak phase is not CKM-suppressed. The ratio of amplitudes is now

$$\lambda_f = \eta_f e^{i2\alpha}\frac{1 - P/Te^{-i\alpha}e^{i\delta}}{1 - P/Te^{+i\alpha}e^{i\delta}} = \eta_f|\lambda_f|e^{i2\alpha_{eff}},$$

where T, P are the magnitudes of the tree and penguin amplitudes and δ their relative strong phase. Since there are three unknowns (α, P/T, and δ) and only two observables ($\mathcal{S}_f$ and $\mathcal{C}_f$), the time-dependent analysis can only measure $\sin 2\alpha_{eff}$ and $|\lambda_f|$ and thus additional information is required to extract α from α_{eff}.

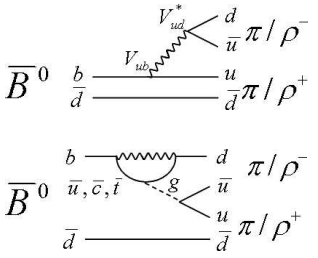

Figure 4. (Top) Tree and (bottom) penguin diagrams contributing to the $B^0 \to \pi^+\pi^-$, $\rho^+\rho^-$, and $\rho^+\pi^-$ decays.

The Gronau and London isospin technique [14] provides the additional information for separating the tree and penguin contributions. Different $B \to hh$ amplitudes can be related through SU(2) isospin symmetry, e.g. $\mathcal{A}^{+0} = 1/\sqrt{2}\mathcal{A}^{+-} + \mathcal{A}^{00}$, or $\overline{\mathcal{A}}^{-0} = 1/\sqrt{2}\overline{\mathcal{A}}^{+-} + \overline{\mathcal{A}}^{00}$, where the superscripts refer to final states h^+h^0, h^+h^-, and h^-h^0, and $\overline{\mathcal{A}}$ denotes the *CP* conjugate amplitude of $\mathcal{A}$. Neutral $B \to h^+h^-$, h^0h^0 decays can have either I=0 or I=2 amplitudes but gluonic penguins only contribute to I=0 (by ΔI=1/2 rule). However, charged $B^+ \to h^+h^0$ decays are pure I=2 with negligible contamination from electroweak penguins (effect on $\alpha \sim 1 - 2^\circ$), and thus only the tree amplitude contributes and $\mathcal{A}^{+0} = \overline{\mathcal{A}}^{-0}$. These isospin relations can be used to constraint the penguin shift $\kappa = 2(\alpha_{eff} - \alpha)$, but requires six samples (four tagged neutral B decays plus two charged), some involving decay channels with small branching fractions. Still, the method has an intrinsic 2-fold ambiguity on $2\alpha_{eff}$, and a 4-fold ambiguity on κ.

The fit to the Δt distribution in $\pi^+\pi^-$ decays yields [15] $\mathcal{S}_{\pi^+\pi^-} = -0.60 \pm 0.11 \pm 0.03$ and $\mathcal{C}_{\pi^+\pi^-} = -0.21 \pm 0.09 \pm 0.02$, implying a significance of *CP* violation above 5 standard deviations. There is still some discrepancy (at 2 standard deviation level) on $\mathcal{C}_{\pi^+\pi^-}$ with the Belle experiment [16]. The isospin analysis in $\pi\pi$ [17] makes use of six different measurements, $\mathcal{S}_{\pi^+\pi^-}$, $\mathcal{C}_{\pi^+\pi^-}$, $\mathcal{C}_{\pi^0\pi^0}$ (i.e. direct *CP* asymmetry in $B^0 \to \pi^0\pi^0$), and the branching ratios for $B^0 \to \pi^+\pi^-$, $B^+ \to \pi^+\pi^0$, and $B^0 \to \pi^0\pi^0$. To extract α, a χ^2 test statistic based on the difference between the predicted values for the six observables and the measured values is first constructed. This χ^2 in then converted into a confidence level (CL) by subtracting the absolute minimum χ^2 value and evaluating the cumulative distribution for one degree of freedom. The resulting 1-CL distribution obtained from this frequentist procedure is shown in Fig. 5(top), from which a value of $\alpha = (96^{+11}_{-6})^\circ$ at 68.3% CL (up to the 8-fold ambiguity) is obtained.

The $B \to \rho^+\rho^-$ channel has the additional complication that it is a $P \to VV$ decay and thus the final state could be a mixture of *CP*-odd and *CP*-even eigenstates. However, it turns out that the decay is almost 100% longitudinally polarized (S- and D-wave). The time-dependent analysis yields [18] $S_{\rho^+\rho^-} = -0.17 \pm 0.20^{+0.05}_{-0.06}$ and

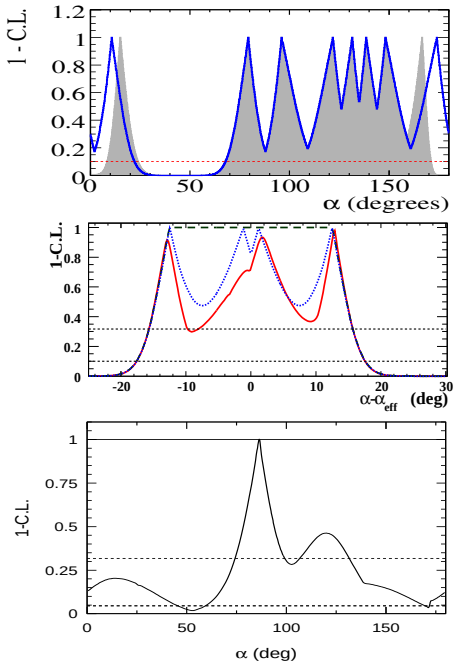

Figure 5. 1-CL vs α obtained from the isospin analysis for (top) $B \to \pi\pi$ and (bottom) $B \to \pi^+\pi^-\pi^0$ decays. (middle) 1-CL vs $\alpha - \alpha_{eff}$ obtained from the isospin analysis for $B \to \rho\rho$ decays. For $\pi\pi$ the shaded area includes SU(3) constraints on penguin amplitude from $B_s \to K^+K^-$ [17]. For $\rho\rho$ the solid line includes all the available information, while the dotted line is the result of the analysis when $\mathcal{S}_{\rho^0\rho^0}$ is excluded, and the dashed line is the result with both $\mathcal{S}_{\rho^0\rho^0}$ and $\mathcal{C}_{\rho^0\rho^0}$ excluded.

$C_{\rho^+\rho^-} = 0.01 \pm 0.15 \pm 0.06$. The isospin analysis in $\rho\rho$ has greatly improved recently with the inclusion of the time-dependent measurement in $\rho^0\rho^0$ using the complete *BABAR* data sample [19], since in this case the availability of proper time information provides a measurement of both $\mathcal{C}$ and $\mathcal{S}$ coefficients, yielding $S_{\rho^0\rho^0} = 0.5 \pm 0.9 \pm 0.2$ and $C_{\rho^0\rho^0} = 0.4 \pm 0.9 \pm 0.2$. Like for $\rho^+\rho^-$, the analysis also measures the longitudinal polarization of the ρ mesons and the branching fraction, $0.70 \pm 0.14 \pm 0.05$ and $0.84 \pm 0.29 \pm 0.17) \times 10^{-6}$, respectively. The signal yield $85 \pm 27 \pm 17$ has a significance of 3.6 standard deviations. As shown in Fig. 5(middle), the constraint from $S_{\rho^0\rho^0}$ helps in reducing the 4-fold ambiguity in the penguin contribution, and favors the solution corresponding to $\alpha - \alpha_{eff} \approx 11^\circ$.

Finally, α can also be extracted from $B \to \rho\pi$ decays. However, in this case the isospin analysis is not viable and a better approach is to perform a time-dependent $\pi^+\pi^-\pi^0$ Dalitz analysis assuming isospin symmetry and that the amplitude is dominated by quasi-two-body decays to $\rho\pi$ and radial excitations [20]. The interference at equal masses (in the corners of the Dalitz plot) provides the information on the relative strong phases. A total of 27 bilinear coefficients of the amplitude, each one related to α and the tree and penguin amplitudes, are measured, from which α can be extracted using a χ^2 (frequentist) method similar to that used in $\pi\pi$ and $\rho\rho$ [21]. The resulting 1-CL distribution is shown in Fig. 5(bottom), from which we obtain $74^\circ < \alpha < 132^\circ$ at 68.3% CL. As it can be observed, this method reduces significantly the ambiguities intrinsic to the isospin analysis.

5. MEASURING γ

The angle γ is experimentally the hardest to measure at *BABAR*. Since γ is the phase of V_{ub} its extraction requires the interference between $b \to c\overline{u}s$ and $b \to u\overline{c}s$ transitions. This can be reached using $B^\pm \to DK^\pm$ decays, where the D meson decays into a final state accessible to both D^0 and $\overline{D}^0$ (see Fig. 6) [22]. Interference between the color-allowed decay $B^+ \to \overline{D}^0 K^+$ and the color-suppressed decay $B^+ \to D^0 K^+$ (and likewise for B^-) gives rise to direct *CP* violation. This approach is theoretically clean since only tree diagrams are involved. Unfortunately, the $b \to u\overline{c}s$ transition is not only color suppressed but also CKM suppressed, thus the ratio r_B between the magnitudes of the two interfering amplitudes is expected to be at 10% level. Since the sensitivity to γ is driven by the ratio r_B, it must be measured as precisely as possible, together with the relative strong phase between the two transitions.

Three different D^0 final states are used to reach

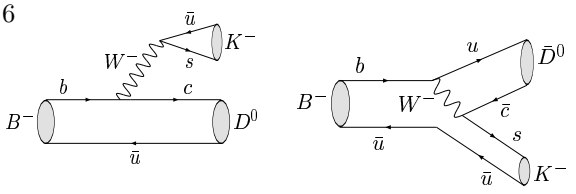

Figure 6. Main diagrams contributing to the $B^- \to DK^-$ decay.

the interference: *CP* eigenstates [23], like $D^0 \to K^+K^-$, $\pi^+\pi^-$, $K^0_S\pi^0$, $K^0_S\phi$, and $K^0_S\omega$; doubly-Cabibbo-suppressed (DCS) modes [24], like $D^0 \to K^+\pi^-$; and 3-body (Dalitz) final states [25], like $K^0_S\pi^+\pi^-$, $K^0_SK^+K^-$, and $\pi^0\pi^+\pi^-$; we use $K^0_Sh^+h^-$ to refer generally to the first two modes. In addition, to increase the sensitivity *BABAR* uses different B decay final states, $B^\pm \to DK^\pm$, $B^\pm \to D^*K^\pm$, and $B^\pm \to DK^{*\pm}$, with $D^* \to D\pi^0, D\gamma$ and $K^{*\pm} \to K^0_S\pi^\pm$.

In the methods based on *CP* and DCS decays the measured observables are overall rates normalized to the flavor specific D decay and direct *CP* asymmetries. For *CP* eigenstates,

$$\mathcal{R}_\pm = \frac{\Gamma(B^- \to D_\pm K^-) + \Gamma(B^+ \to D_\pm K^+)}{[\Gamma(B^- \to D^0K^-) + \Gamma(B^+ \to \overline{D}^0K^+)]/2},$$
$$\mathcal{A}_\pm = \frac{\Gamma(B^- \to D_\pm K^-) - \Gamma(B^+ \to D_\pm K^+)}{\Gamma(B^- \to D_\pm K^-) + \Gamma(B^+ \to D_\pm K^+)}.$$

These observables can be related to the fundamental parameters, γ, r_B, and the relative strong phase δ_B, $\mathcal{R}_\pm = 1 + r_B^2 + \pm 2r_B\cos\delta_B\cos\gamma$ and $\mathcal{A}_\pm = \pm 2r_B\sin\delta_B\sin\gamma/\mathcal{R}_\pm$, with $\mathcal{A}_+\mathcal{R}_+ = -\mathcal{A}_-\mathcal{R}_-$. The measurements of $\mathcal{R}$ and $\mathcal{A}$ from *CP* and DCS decay channels alone do not allow to constraint γ (for *CP* eigenstates there is an 8-fold ambiguity while for DCS final states there are more unknowns than observables), but help to constrain γ in combination with the Dalitz method, as discussed below.

BABAR has recently updated the *CP* analyses using $B^\pm \to DK^\pm$ and $B^\pm \to D^*K^\pm$ decays. The $B^\pm \to DK^\pm$ analysis [26] yields $\mathcal{R}_+ = 1.06 \pm 0.10 \pm 0.05$, $\mathcal{R}_- = 1.03 \pm 0.10 \pm 0.05$, $\mathcal{A}_+ = 0.27 \pm 0.09 \pm 0.04$, and $\mathcal{A}_- = -0.09 \pm 0.09 \pm 0.02$. Similarly, the $B^\pm \to D^*K^\pm$ analysis [27] gives $\mathcal{R}^*_+ = 1.31 \pm 0.13 \pm 0.04$, $\mathcal{R}^*_- = 1.10 \pm 0.12 \pm 0.04$, $\mathcal{A}^*_+ = -0.11 \pm 0.09 \pm 0.01$, and $\mathcal{A}^*_- = +0.06 \pm 0.10 \pm 0.02$. Note the 2.8 standard deviation significance of the direct *CP* asymmetry observed for *CP*-even $B^\pm \to DK^\pm$ decays, reflecting the difference in the number of signal $B^- \to DK^-$ (149) and $B^+ \to DK^+$ (106) decays.

In the 3-body $K^0_Sh^+h^-$ final states the angle γ is extracted through an analysis of the distribution of the events in the D^0 Dalitz plane. The D^0 to 3-body decay dynamics insures the presence of a strong charm decay phase varying over the Dalitz plot, and thus the interference at equal masses provides the information for a simultaneous determination of γ and the B decay strong phase δ_B (up to only a 2-fold ambiguity, mod 180°), and r_B. Neglecting effects from $D^0 - \overline{D}^0$ mixing and *CP* asymmetries in neutral D decays (which are negligible), the $B^\pm \to DK^\pm$, $D \to K^0_Sh^+h^-$ decay rate can be written as

$$\Gamma_\pm(m^2_-, m^2_+) \propto |\mathcal{A}_{D\pm}|^2 + r_B^2|\mathcal{A}_{D\mp}|^2 + 2\lambda\left[x_\pm\Re\{\mathcal{A}_{D\pm}\mathcal{A}^*_{D_\mp}\} + y_\pm\Im\{\mathcal{A}_{D\pm}\mathcal{A}^*_{D\mp}\}\right],$$

where $x_\pm = \kappa r_B\cos(\delta_B \pm \gamma)$ and $y_\pm = \kappa r_B\sin(\delta_B \pm \gamma)$ (i.e. the real and imaginary parts of the ratio of $b \to u\bar{c}s$ and $b \to c\bar{u}s$ amplitudes) are the so-called Cartesian *CP* parameters [28], where $x_\pm^2 + y_\pm^2 = r_B^2$. These are the *CP* parameters experimentally determined, since in terms of these observables the likelihood behaves Gaussian and unbiased. Here, $m^2_\pm \equiv m^2(K^0_Sh^\pm)$, $\mathcal{A}_{D\pm} \equiv \mathcal{A}_D(m^2_\pm, m^2_\mp)$, with $\mathcal{A}_{D+} = \mathcal{A}(\overline{D}^0 \to K^0_Sh^-h^+)$ and $\mathcal{A}_{D-} = \mathcal{A}(D^0 \to K^0_Sh^+h^-)$. Similar relations hold for $B^\pm \to D^*K^\pm$ and $B^\pm \to DK^{*\pm}$ decays. The factor λ accounts for the different parity of $B^\pm \to D^*[D\gamma]K^\pm$ with respect to all other decays, while the parameter $0 < \kappa < 1$ accounts for the effects consequence of the natural width of the K^*.

A model is required to describe the $\mathcal{A}_{D\pm}$ decay amplitude. This model is obtained from an independent analysis of a high statistics pure sample of $D^{*+} \to D^0\pi^+$ decays from $c\bar{c}$ production, where the D^0 flavor is tagged using the charge of the D^* meson. In the recent analysis, *BABAR* uses D^0 mesons decaying into $K^0_S\pi^+\pi^-$, and for the first time, $K^0_SK^+K^-$ [29]. The $D^0 \to K^0_S\pi^+\pi^-$ model employs 9 Breit-Wigner resonances to describe the P and D wave dynamics, while for the

$\pi\pi$ S-wave a K-matrix formalism is used instead to deal with the broad, overlapping and multi-channel scalar resonances. The $K\pi$ S-wave is described using a parameterization corresponding to a K-matrix approach describing a rapid phase shift coming from a resonant term (corresponding to a $K_0^*(1430)^-$ Breit-Wigner) and a slow rising phase shift governed by a non-resonant term. Similarly, the $D^0 \to K_S^0 K^+ K^-$ model uses an standard Breit-Wigner approach with 8 resonances.

Figure 7 shows the 39.3% and 86.5% $(x_\pm, y_\pm)$ 2-dimensional confidence-level contours, corresponding to one- and two-standard deviation regions, for $B^\pm \to DK^\pm$ and $B^\pm \to D^*K^\pm$ decays. Similar contours are obtained for $B^\pm \to DK^{*\pm}$ decays. The radial separation between the regions for B^+ and B^- decays is just $2r_B|\sin\gamma|$, while the angular separation is 2γ. These results can be converted into a CL as a function of γ using a frequentist χ^2 method essentially identical to that used for α (see Fig. 8), yielding $\gamma = (76^{+23}_{-24})^\circ$ at 68.3% CL, including all errors. The contribution to the total error due to experimental and Dalitz model systematic uncertainties, amounting to 5° each, are almost negligible compared to the statistical error. The strong phases and the ratios r_B for the different B decay modes are determined similarly. For the r_B ratios *BABAR* obtains $r_{B\to DK} = 0.086 \pm 0.035$, $r_{B\to D^*K} = 0.135 \pm 0.051$, and $r_{B\to DK^*} = 0.18^{+0.10}_{-0.12}$, which provide the most stringent constraints from a single measurement to date. These results imply a combined significance of direct *CP* violation (i.e. $\gamma \neq 0$) of 3.0 standard deviations. Note that the key r_B ratios for $B^\pm \to DK^\pm$ and $B^\pm \to D^*K^\pm$ are well above 2 standard deviations away from zero.

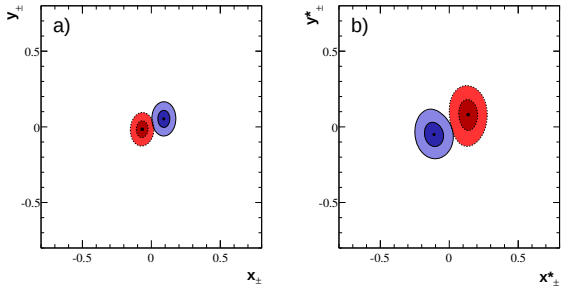

Figure 7. Contours at 39.3% (dark) and 86.5% (light) 2-dimensional confidence-level (CL) in the $(x_\pm, y_\pm)$ plane (statistical only), for (a) $B^\pm \to DK^\mp$ and (b) $B^\pm \to D^*K^\pm$, for B^- (thick and solid lines) and B^+ (thin and dotted lines) decays.

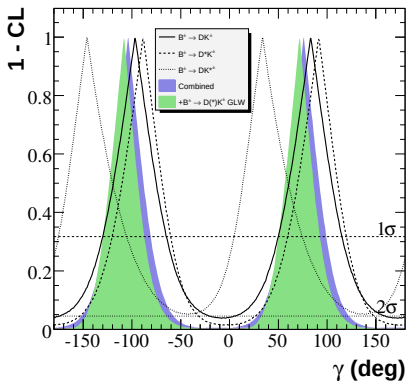

Figure 8. 1-CL as a function of γ from the 3-body (Dalitz) analysis of $K_S^0 h^+ h^-$ final states, for $B^\pm \to DK^\pm$, $B^\pm \to D^*K^\pm$, and $B^\pm \to DK^{*\pm}$ decays separately, and their combination. The combination with the updated $B^\pm \to DK^\pm$ and $B^\pm \to D^*K^\pm$ analysis using *CP* decays is also shown.

6. SUMMARY AND CONCLUSION

In summary, the measurement of $\sin 2\beta$ in $b \to c\bar{c}s$ transitions (e.g. $B^0 \to J/\psi K^0$ decays) at *BABAR* has reached a precision of 0.035 (2%), which translates to $\sim 1.4^\circ$ uncertainty on β, approaching the accuracy of SM calculations (0.1-1%). All β measurements in a variety of channels involving $b \to c\bar{c}d$, $b \to d\bar{d}s$, and $b \to s\bar{s}s$ transitions, the latter being particularly sensitive to new physics contributions, are consistent with the reference from charmonium decays.

The measurement of α relies on the analysis of $b \to u\bar{u}d$ transitions in $B \to \pi\pi$, $\rho\rho$, and $\rho\pi$ decays. All these decay modes provide consistent and complementary results, which help in reducing ambiguities and uncertainties due to the penguin pollution. The 1-CL distribution ob-

tained combining all the available *BABAR* information is shown in Fig. 9, from which we obtain $\alpha = (83.5^{+13.5}_{-5.7})^\circ$.

Finally, the angle γ is the most difficult to measure and now is being determined using $B^\pm \to D^{(*)}K^{(*)\pm}$ decays with an uncertainty of about 20°, dominated by the Dalitz method. The 1-CL distribution as a function of γ obtained combining the recent *BABAR* results using D^0 decays into *CP* and 3-body ($K^0_S\pi^+\pi^-$ and $K^0_SK^+K^-$) final states is shown in Fig. 8, yielding $\gamma = (72^{+21}_{-22})^\circ$, with ratios $r_{B\to DK} = 0.090^{+0.028}_{-0.027}$, $r_{B\to D^*K} = 0.113^{+0.057}_{-0.046}$, and $r_{B\to DK^*} = 0.19^{+0.10}_{-0.11}$.

All the measurements of the three angles are statistically limited (particularly γ and α), and are consistent with the SM predictions. The analysis of the complete data sample, the addition of new channels (e.g. $B \to a_1\pi$), and their combination could yet improve the constraint on α and γ.

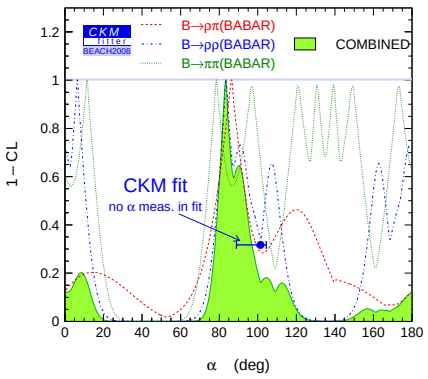

Figure 9. Global *BABAR* 1-CL vs α using $B \to \pi\pi$, $\rho\rho$, and $\rho\pi$ decays [31].

REFERENCES

1. Slides: http://beach2008.sc.edu/includes/documents/sessions/martinez-vidal.talk.pdf
2. N. Cabibbo, Phys. Rev. Lett. **10**, 531 (1963); M. Kobayashi and T. Maskawa, Prog. Theor. Phys. **49**, 652 (1973).
3. L. Wolfenstein, Phys. Rev. Lett. **51**, 1945 (1983).
4. B. Aubert *et al.*, Nucl. Instrum. Methods Phys. Res., Sect. A **479**, 1 (2002).
5. In the following, all cites to *BABAR* articles will omit "B. Aubert *et al.*".
6. R. Fleischer, J. Phys. G **32** (2006); H. Boos, T. Mannel and J. Reuter, Phys. Rev. D **70**, 036006 (2004); H.-n. Li and S. Mishima, JHEP **0703** (2007) 009.
7. Phys. Rev. Lett. **94**, 161803 (2005).
8. Phys. Rev. Lett. **99**, 171803 (2007).
9. M. Beneke, Phys. Lett. B **620**, 143 (2005); H.-Y. Cheng, Ch.-K. Chua, and A. Soni, Phys. Rev. D **72**, 014006 (2005).
10. Phys. Rev. Lett. **101**, 021801 (2008).
11. M. Ciuchini, M. Pierini, and L. Silvestrini, Phys. Rev. Lett. **95**, 221804 (2005).
12. Phys. Rev. D **76**, 111102 (2007).
13. HFAG, http://www.slac.stanford.edu/xorg/hfag/
14. M. Gronau and D. London, Phys. Rev. Lett. **65**, 3381 (1990).
15. Phys. Rev. Lett. **99**, 021603 (2007).
16. H. Ishino *et al.*, Phys. Rev. Lett. **98**, 211801 (2007).
17. Phys. Rev. D **76**, 091102 (2007).
18. Phys. Rev. D **99**, 052007 (2007).
19. arXiv:0708.1630 [hep-ex].
20. A. E. Snyder and H. R. Quinn, Phys. Rev. D **48**, 2139 (1993).
21. Phys. Rev. D **76**, 012004 (2007).
22. M. Gronau, Phys. Lett. B **557**, 198 (2003);
23. M. Gronau and D. London, Phys. Lett. B **253**, 483 (1991); M. Gronau and D. Wyler, Phys. Lett. B **265**, 172 (1991).
24. D. Atwood, I. Dunietz and A. Soni, Phys. Rev. Lett. **78**, 3257 (1997); Phys. Rev. D **63**, 036005 (2001).
25. A. Giri, Y. Grossman, A. Soffer and J. Zupan, Phys. Rev. D **68**, 054018 (2003).
26. Phys. Rev. D **77**, 111102(R) (2008).
27. arXiv:0807.2408 [hep-ex].
28. Phys. Rev. Lett. **95**, 121802 (2005).
29. Phys. Rev. D **78**, 034023 (2008).
30. D. Aston *et al.*, Nucl. Phys. B **296**, 493 (1988).
31. J. Charles *et al.*, Eur. Phys. J C **41**, 1 (2005).